The FORS Deep Field: Photometric Data and Photometric Redshifts

R. Bender[1], I. Appenzeller[2], A. Böhm[2], N. Drory[1], K.J. Fricke[3], A. Gabasch[1], J. Heidt[2], U. Hopp[1], K. Jäger[3], M. Kümmel[2], D. Mehlert[2], C. Möllenhoff[2], A. Moorwood[4], H. Nicklas[3], S. Noll[2], R.P. Saglia[1], W. Seifert[2], S. Seitz[1], O. Stahl[2], E. Sutorius[2], T. Szeifert[5], S.J. Wagner[2], and B.L. Ziegler[3]

[1] Universitäts-Sternwarte, Scheinerstr.1, D–81679 München, Germany
[2] Landessternwarte Heidelberg, Königstuhl, 69117 Heidelberg, Germany,
[3] Universitäts-Sternwarte, Geismarlandstr.11, D–37083 Göttingen, Germany
[4] European Southern Observatory, D-85748 Garching b. München, Germany
[5] European Southern Observatory, Alonso de Cordova 3107 Santiago 19, Chile

Abstract. Deep multicolor fields are an important tool to explore the formation and evolution of galaxies out to the highest redshifts and faintest magnitude limits (Ferguson et al. [11]). This is also the aim of the FORS Deep Field (FDF), which has about 5 times the field-size of the two Hubble Deep Fields together and, in addition, contains a relatively bright quasar of 18.5mag at $z = 3.36$ at its center. A full exploration of the FDF multicolor data requires good photometric redshifts. In this paper we provide an overview of the data, describe our photometric redshift technique and present the redshift distribution in the FDF.

1 The FDF Photometric Data

The FORS Deep field is centered on the QSO Q0103-260 at $z = 3.36$ with α_{2000} =01^{h}06^{m}03.6^s, δ_{2000} =-25^{o}45'46". For details on the selection criteria, see Appenzeller et al. [1], Heidt et al. [14].

Table 1 gives the filters used, their corresponding exposure times, seeing values and the limiting magnitudes (preliminary) reached. The broadband observations were carried out in Bessel U B R I filters and Gunn g and z bands. Narrow band observations were obtained at the redshifted Lyα line of the quasar and its blueward continuum.

Unfortunately, during the FDF observing periods, the seeing on Paranal was worse than average and, in addition, the telescope had significantly reduced efficiency (presumably due to degrading of the primary mirror coating). Therefore, the original goals in image quality and depths could not be achieved fully. The following numbers of galaxies were detected (for the field sizes in Table 1): B-band: $\sim$ 4100 to $\mathrm{m_B}$ = 27.5, R-band: $\sim$ 5100 to $\mathrm{m_R}$ = 26.75, and I-band: $\sim$ 4600 to $\mathrm{m_I}$ = 26.25.

Finally, the FORS observations were supplemented with imaging in J and K bands using SofI at the NTT.

Table 1. Observing Log of the FORS Deep Field Imaging Observations

Filter	Exp.Time [hours]	Seeing [arcsec]	Field-of-View [arcmin^2]	Completeness (5 σ) [mag]
U	10.7	1.15	6.2 × 6.4	25.50
B	4.4	0.95	5.8 × 5.8	27.50
g	5.0	1.00	6.3 × 6.4	27.00
R	5.8	0.85	6.4 × 6.4	26.75
I	4.0	0.60	6.1 × 5.8	26.25
z	3.5	0.75	6.8 × 6.8	t.b.d.
530_25	4.0	0.80	6.8 × 6.8	t.b.d.
485_37	3.0	0.85	6.8 × 6.8	t.b.d.
J (SofI)	1.7	0.80	6.8 × 7.9	22.50
K (SofI)	1.7	0.75	6.8 × 7.9	20.50

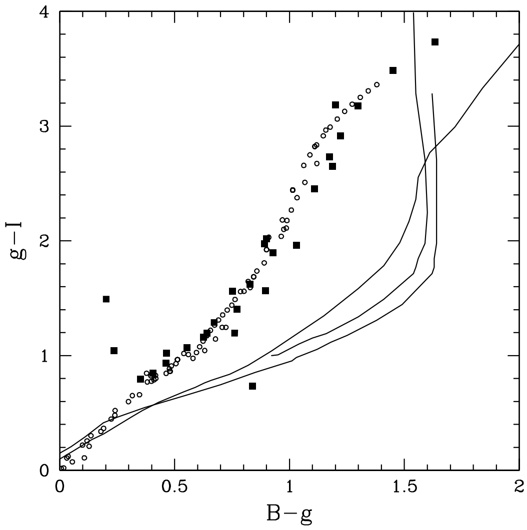

Fig. 1. The B-g vs. g-I color-color diagram of stars detected in the FDF (big filled squares), compared with the expected color-color sequence as derived from the convolution of the total (VLT+FORS+CCD) filter efficiency curves with the Bruzual-Persson-Gunn-Stryker library of standard stars (small open circles). These colors are in the FORS filter system. For comparison, the standard Johnson-Kron-Cousins colors B-V vs. V-I of main sequence stars, giants and supergiants are shown as lines.

We checked the accuracy of the FDF photometry via a comparison of the observed stellar sequences in the color-color-diagrams with the expected synthetic sequences obtained from the convolution of the total filter transmission curves (VLT+FORS+CCD) with the stellar library of Bruzual-Persson-Gunn-Stryker (updated version of the Gunn-Stryker atlas [13], from STScI homepage [7]). From Fig. 1 it is evident that both the color zeropoints and the curvature of the B-g vs. g-I color-color sequence are well matched. The latter is sensitively dependent on the correct total filter transmission curves. The comparison with the Johnson-Kron-Cousins colors of main sequence stars, giants and supergiants ([15], full lines in Fig. 1) illustrates the non-linearity of the color transformation between the FDF colors and the standard system.

Our experiments with the photometric data show that even rather minor zeropoints offsets or badly determined color-terms (in case one attempts to transform to the standard Johnson-Kron-Cousins system) can cause significant errors in the photometric redshift distribution (see also the discussion in [4]. In order to obtain unbiased photometric redshifts it is important to work in the instrument system (avoiding non-linear color transformations) and to check the photometric zeropoints with synthetic sequences of standard stars.

2 The Photometric Redshift Technique

Our photometric redshift technique follows a Baysian approach and is similar to the one of Benitez [3]. It uses optionally either template spectra or a fitted combination of eigenspectra (like in Connolly et al. [10]) to determine the full redshift probability function for each object. Details of the method can be found in Bender and Gabasch [2].

The set of template spectra was derived from the Hubble Deep Field North (Williams et al. [20]) using objects with known spectroscopic redshifts. These were grouped into classes of similar values for (a) the Balmer or 4000A break, (b) UV to optical flux, and (c) near IR to optical flux. This produced about 20 independent spectral-energy-distributions (SEDs). In order to obtain our final templates, each one of these empirical broad-band SEDs was fitted by a combination of up to 8 simple stellar population models of different ages from Maraston [18]. Extinction was allowed to vary for each of the components and was assumed to follow a Calzetti et al. law [8]. In this way, our final templates have broad-band energy-distributions compatible with real galaxies but much higher spectral resolution of about 10Å. The latter is important if medium-band or narrow-band filters are to be included in the photometric redshift determination. A subset of our semi-empirical templates is shown in Figure 2.

For the the calculation of the redshift probability function, the templates were corrected for Lyman forest absorption following Madau [17]. As a check, we compared our photometric redshifts with the spectroscopic ones in the central Hubble Deep Field North and found excellent agreement (spectroscopic redshifts courtesy M. Dickinson, photometric data from [12]). Only for one out of 108 objects the photometric redshift was completely off ($z_{spec} = 2.9$, $z_{phot} = 0.2$). For all other objects the relative error in z was smaller than about 0.2. The median value in the residuals $(z_{phot} - z_{spec})/(1 + z_{spec})$ was calculated to be 0.033.

Note that our procedure to derive semi-empirical templates from broad-band photometric data differs from most methods used so far, which either

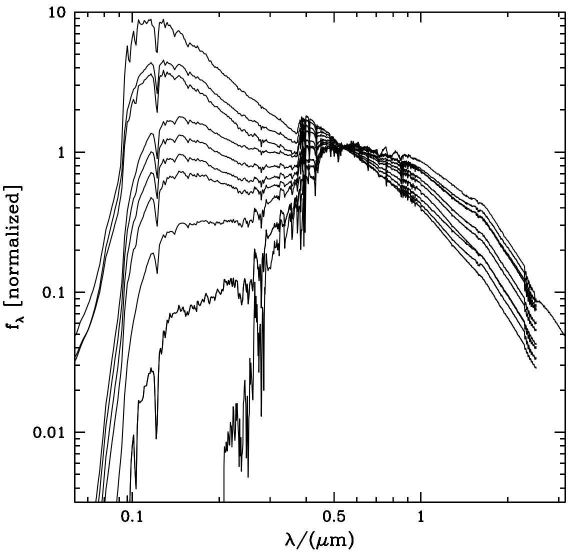

Fig. 2. A selection of semi-empirical spectral energy distributions derived from galaxies with spectroscopic redshifts in the Hubble Deep Field North (see text for details). These templates and several more of intermediate type are used in our photometric redshift technique as the template set.

use completey empirical templates, like the ones from Coleman et al. [9] (which have relatively low resolution and need extrapolation in wavelength [12] as well as iterative optimization of their shapes [5]), or, model templates from, e.g., Bruzual and Charlot [6] used by, e.g., the Bolzonella et al. method [4].

We finally determined the eigenspectra of these high-resolution semi-empirical templates which proved to be similar to those of Connolly et al. [10]. In the results shown here we only made use of the original templates, not of the optimal combination of eigenspectra for each object.

3 Photometric Redshifts and Redshift Distribution

Using these semi-empirical templates, we derived photometric redshifts for the Fors Deep Field objects. A comparison between spectroscopic and photometric redshifts for the FDF is shown in Fig. 3. Despite of a less broad wavelength coverage in the FDF than in the Hubble Deep Fields, we obtain very satisfactory results. Only 2 out of 73 objects with reliable spectroscopic redshifts have mismatching photometric redshifts. This fraction is small enough to not distort the derivation of luminosity densities and star formation histories significantly.

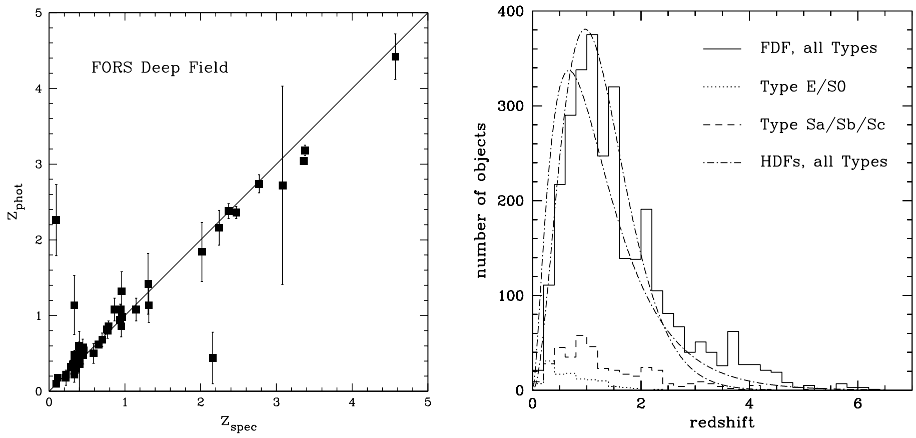

Fig. 3. Left: Photometric vs. spectroscopic redshifts in the FORS Deep Field. The median residual in $(z_{phot} - z_{spec})/(1 + z_{spec})$ is 0.042. **Right:** Distribution of photometric redshifts in the FORS Deep Field. For comparison the photometric redshift distributions in the Hubble Deep Fields North and South are shown schematically as dot-dashed lines.

The photometric redshift distribution for the sub-area of the FDF where good photometry was available in all filters is shown in Fig. 3. For comparison the redshift distributions of the Hubble Deep Fields North and South are indicated as well. It is evident that, though the distributions are similar, significant cosmic variance still exists between the redshift distributions of these three fields. For the FORS deep field, we also show type-dependent redshift distributions. Early-type spectra basically disappear beyond $z \approx 1.5$, spiral-type spectra are still found to $z \approx 2.5$, while irregular and starburst spectra are the most frequent types at all redshifts beyond $z \approx 0.5$. The redshift distribution of the E/SO types shows a peak at $z \approx 0.3$. It corresponds to a galaxy cluster which is easily visible in the FORS images but was not evident in the Digitized Sky Survey Images from which the field was selected.

4 Outlook

The observations for the FORS deep field started somewhat more than a year ago. By now, in addition to the imaging data, about 100 spectra have been analysed and some 200 more have recently been obtained (Mehlert et al. [19]). The imaging data are almost fully reduced and calibrated, galaxy counts and correlation functions have been analysed (Kümmel et al. [16]) and photometric redshifts were calculated as described above. We are now in the process of carrying through our main science projects. A few examples are:

- The Tully-Fisher relation of field spirals at $z = 0.2...1$.
- Analysis of the quasar host galaxy, its environment and Lyα absorbers.
- Luminosity densities of galaxies and star formation history.
- Dark matter properties of galaxies from galaxy-galaxy lensing.

Acknowledgements. We thank the Paranal and La Silla staff for efficient support of the observations. Our work was funded by the Deutsche Forschungsgemeinschaft (SFB 375, SFB 439), the VW foundation and the German Federal Ministry for Education and Science (ID-Nos. 05 2HD50A, 05 2GO20a and 05 2MU104).

References

1. Appenzeller, I. et al. (2000), From Extrasolar Planets to Cosmology: The VLT Opening Symposium, Eds. J. Bergeron & A. Renzini, Springer Berlin, p3
2. Bender, R., Gabasch. A. (2001) in preparation
3. Benitez, N. (1999) ASP Conf. Ser. **191**, 31
4. Bolzonella, M., Miralles, J.-M., Pello, R. (2000), A&A **363**, 476
5. Budavari, T. et al. (2000) AJ **120**, 1588
6. Bruzual-Charlot galaxy library: `www.stsci.edu/instruments/observatory/cdbs/astronomical_catalogs`
7. Bruzual-Persson-Gunn-Stryker stellar atlas: `www.stsci.edu/instruments/observatory/cdbs/astronomical_catalogs`
8. Calzetti, D., Kinney, A.L., Storchi-Bergmann, T. (1994) ApJ **429**, 582
9. Coleman, G.D., Wu, C.C., Weedman, D.W. (1980), ApJS **43**, 393
10. Connolly, A.J., Szalay, A.S., Bershady, M.A., Kinney, A.L., Calzetti, D. (1995), AJ **110**, 1071
11. Ferguson, H., Dickinson, M., Williams, R. (2000) AARA **38**, astro-ph 0004319, in press
12. Fernandez-Soto, A., Lanzetta, K., Yahil, A. (1999), ApJ **513**, 34
13. Gunn, J.E., Stryker, L.L. (1983) ApJS **52**, 121
14. Heidt, J. et al. (2001) Rev. Mod. Astron. **14**, in press
15. Johnson, H.L. (1966) ARAA **4**, 193
16. Kümmel. M. et al. (2001) this conference
17. Madau, P. (1995) ApJ **441**, 18
18. Maraston, C. (1998) MNRAS **300**, 872
19. Mehlert, D. et al. (2001) this conference
20. Williams, R.E. et al. (1996) AJ **112**, 1335